Sciencexpress Reports

Covalent organic frameworks comprising cobalt porphyrins for catalytic CO_2 reduction in water

Song Lin,[1,2]* Christian S. Diercks,[1,3]* Yue-Biao Zhang,[1,3,4]* Nikolay Kornienko,[1] Eva M. Nichols,[1,2] Yingbo Zhao,[1] Aubrey R. Paris,[1] Dohyung Kim,[5] Peidong Yang,[1,3,5,6] Omar M. Yaghi,[1,3,6,7]† Christopher J. Chang[1,2,8,9]†

[1]Department of Chemistry, University of California, Berkeley, CA 94720, USA. [2]Chemical Sciences Division, Lawrence Berkeley National Laboratory, Berkeley, CA 94720, USA. [3]Materials Sciences Division, Lawrence Berkeley National Laboratory, Berkeley, CA 94720, USA. [4]School of Physical Science and Technology, ShanghaiTech University, Shanghai, 201210, China. [5]Department of Materials Science and Engineering, University of California, Berkeley, CA 94720, USA. [6]Kavli Energy Nanoscience Institute, Berkeley, CA 94720, USA. [7]King Fahd University of Petroleum and Minerals, Dhahran 34464, Saudi Arabia. [8]Howard Hughes Medical Institute, University of California, Berkeley, CA 94720, USA. [9]Department of Molecular and Cell Biology, University of California, Berkeley, CA 94720, USA.

*These authors contributed equally to this work.

†Corresponding author. E-mail: yaghi@berkeley.edu (O.M.Y.); chrischang@berkeley.edu (C.J.C.)

Conversion of carbon dioxide to carbon monoxide and other value-added carbon products is an important challenge for clean energy research. Here, we report modular optimization of covalent organic frameworks (COFs), in which the building units are cobalt porphyrin catalysts linked by organic struts through imine bonds, to prepare a catalytic material for aqueous electrochemical reduction of CO_2 to CO. The catalysts exhibit high Faradaic efficiency (90%) and turnover numbers (up to 290,000 with initial turnover frequency 9400 hours^{-1}) at pH 7 with an overpotential of –0.55 V, equivalent to a 60-fold improvement in activity compared to the molecular cobalt complex, with no degradation over 24 hours. X-ray absorption data reveal the influence of the COF environment on the electronic structure of the catalytic cobalt centers.

Global energy demands and climate change underpin broad interest in the sustainable reductive transformation of carbon dioxide (CO_2) to value-added carbon products like carbon monoxide (CO) (*1*, *2*). Electrolytic approaches benefit from using water as the reaction medium, as it is a cheap, abundant, and environmentally benign solvent that facilitates proton and electron transfer (*3*, *4*); however, the competitive and often kinetically favored off-pathway reduction of water itself to hydrogen must be avoided. In this context, molecular catalysts for electrochemical CO_2 conversions can be systematically tuned to achieve high activity and selectivity over proton reduction (*5*–*13*), but typically require organic media to achieve optimal selectivity and/or stability, often to maximize solubility and minimize water/proton-induced catalyst degradation an/or hydrogen production. In contrast, heterogeneous catalysts are often stable in water, but optimizing their activity through structural changes at a molecular level remains a substantial challenge (*14*–*19*). Against this backdrop, we sought to investigate crystalline porous frameworks, specifically covalent organic frameworks (COFs) (*20*–*22*), as tunable materials for electrocatalysis. We reasoned that such materials could potentially combine advantages of both molecular and heterogeneous catalysts: (i) construction with molecular building blocks would enable precise manipulation of the spatial arrangement of catalytic centers within the predetermined COF structure (*23*); (ii) the frameworks could be expanded and functionalized without changing the underlying topology of the structure (*24*, *25*); (iii) the conserved pore environment around the active sites within the COF could be tuned electronically and sterically (*26*) while providing ready access for the substrate (*27*–*32*) (Fig. 1). Moreover, these crystalline porous frameworks offer the possibility to perform multivariate synthesis, in which topologically identical and yet functionally modified building blocks can be introduced into the structure. This approach can potentially give rise to materials with emergent properties that are greater than the sum of the individual molecular parts because one can predictably prepare a topologically ordered framework yet introduce heterogeneity in the number and ratio of functionalities by choice of building blocks (*33*). Here we show that incorporation of catalytic cobalt porphyrin (*34*) units into COFs, along with multivariate synthesis of frameworks bearing catalytic cobalt and structural copper units, gives highly active, stable, and selective catalysts for electrochemical reduction of carbon dioxide to carbon monoxide in water. A member of the COF series studied exhibits 60-fold increase in activity compared to the parent molecular precursor and, in many respects, outperforms state-of-the-art molecular and solid-state catalysts, with broad opportunities for further improvement through modular synthesis using appropriate combinations of building units. X-ray absorption measurements reveal that the COF framework can directly influence the electronic structure of the catalytic cobalt centers, in a manner akin to redox non-innocent ligand behavior observed in molecular systems (*35*), thereby contributing to

Downloaded from www.sciencemag.org on August 30, 2015

the observed gains in reaction selectivity and activity beyond the steric effects of surface area and site isolation.

We focused our initial electrocatalysis studies on COFs, as we sought to exploit the charge-carrier mobility of these materials derived from π conjugation and π–π stacking (*22*, *36–38*) and stability from reticular assembly with strong covalent bonds. A model framework COF-366-Co was synthesized by the imine condensation of 5,10,15,20-tetrakis(4-aminophenyl)porphinato]cobalt [Co(TAP)] with 1,4-benzenedicarboxaldehyde (BDA) (Fig. 1). The porous COF material was evacuated by activation with supercritical carbon dioxide and heating to 100°C for 18 hours. The retention of cobalt in the coordinating porphyrin units within the framework was confirmed by elemental analysis (section S1.1), thermogravimetric analysis (TGA) (fig. S1) and solid-state UV-Vis spectroscopy (fig. S3). The formation of the imine linkages in the COF was confirmed by attenuated total reflectance Fourier-transform infrared spectroscopy (ATR-FTIR), which showed the characteristic imine stretching vibration band at 1621 cm^{-1} and the absence of the aldehyde stretching vibration band at 1684 cm^{-1} (fig. S10). The morphologies of the activated COF samples were examined by scanning electron microscopy (SEM), which showed aggregation of only one kind of crystallite of rectangular rod-shaped morphology (ca. 50 nm in length; Fig. 2A). Powder X-ray diffraction (PXRD) patterns (Fig. 2B) showed intense peaks in the expected low-angle range with no residual peaks characteristic of the starting materials. To elucidate the constitution of the framework, we constructed a structural model (Fig. 1) using Materials Studio 7.0 in an orthorhombic *Cmmm* space group to allow the lattice distortion from regular square nets. Pawley refinements of the PXRD patterns were carried out for full profile fitting against the proposed models resulting in a good agreement factor (R_{wp} = 2.59% and R_p = 1.38% after convergence) and reasonable profile differences. These refinements revealed one-dimensional channels running along the *c*-axis of 21 Å in width, with a distance between the stacking two-dimensional sheets of 4.4 Å. The porosity and specific surface area were determined using nitrogen adsorption isotherms at 77 K (Fig. 2C). The BET surface area was determined as 1360 m^2/g. DFT fitting of the adsorption branches showed relatively narrow pore size distributions (10 to 18 Å) in agreement with that of the proposed model.

For electrochemical experiments, the activated microcrystalline COF powders were deposited on porous, conductive carbon fabric. Cyclic voltammetry (CV) measurements on COF-366-Co were conducted in pH 7 aqueous phosphate buffer (Fig. 3A). Under a nitrogen atmosphere, the voltammogram trace shows a departure from the electrode background at about −0.45 V vs. reversible hydrogen electrode (RHE), and a broad reduction wave at about −0.67 V, which was assigned to the Co^{II}/Co^{I} redox couple. The surface concentration of electrochemically active cobalt porphyrin sites was measured by integration of the reduction wave to be 1 × 10^{-8} mol/cm^2, corresponding to activity at 4% of the cobalt porphyrin sites in the material. The observed continuous current increase at potentials more negative than −0.67 V likely arises from Co(I)-catalyzed proton reduction activity (*39*). After the solution was saturated with carbon dioxide, a significant current enhancement was observed (catalytic current/noncatalytic current ratio i_{cat}/i_p = 1.8 at −0.67 V) (*40*), with a catalytic onset potential at −0.42 V, indicating a prominent catalytic effect of COF-366-Co on the reduction of carbon dioxide in neutral aqueous solution. In contrast, the carbon fabric electrode alone showed minimal current enhancement under a carbon dioxide or nitrogen atmosphere (fig. S56).

In controlled potential electrolyses performed in carbon dioxide-saturated aqueous bicarbonate buffer (pH = 7.3) under applied potentials between −0.57 V and −0.97 V (versus RHE), carbon monoxide was observed as the major reduction product (Fig. 3B) with no other detectable carbon-based products; at −0.67 V, which represents a −0.55 V overpotential, the catalyst displayed optimal performance (figs. S63 and S64). More positive potentials led to sluggish carbon dioxide reactivity, whereas more negative potentials promoted off-pathway water reduction. At −0.67 V, COF-366-Co promoted carbon monoxide evolution at an initial current density of 5 mA/mg catalyst (ca. 80 mA/mg cobalt) with high selectivity over competing proton reduction (Faradaic efficiency for carbon monoxide, FE_{CO} = 90%). Catalytic cobalt porphyrin centers in the COF showed greater than 10% enhancement in carbon dioxide to proton selectivity over the molecular cobalt porphyrin unit alone (Fig. 3B). The catalytic activity of the COF could be maintained for 24 hours, accumulating more than 36 ml carbon monoxide (STP, equivalent to 1.6 mmol) per mg COF, corresponding to a turnover number (TON) of 1352 (TON per electroactive cobalt based on the measurements described above, TON_{EA} ≈ 34,000), with an initial turnover frequency (TOF) of 98 $hours^{-1}$ (TOF per electroactive cobalt, TOF_{EA} ≈ 2500). This result represents a significant improvement over the molecular Co(TAP), which showed an initial TOF of 36 $hours^{-1}$ (TOF_{EA} ≈ 360) and a TON of 794 (TON_{EA} ≈ 8,300) after 24 hours of reaction (surface coverage of electroactive sites on Co(TAP)-modified electrode constitutes ca. 10% of the total cobalt). PXRD (fig. S73) and SEM (fig. S74) measurements on the COF catalyst after electrolysis showed neither marked changes in crystallinity and microscopic morphology nor evidence of cobalt nanoparticle formation. By incorporating this molecular unit into a COF scaffold, the resulting hybrid catalyst could be recovered from the electrolysis mixture and reused at least five times without decrease in activity and selectivity (table S8). Control experiments with COFs containing either free-base or copper-metallated porphyrin units, a physical mixture of independently synthesized cobalt nanoparticles (fig. S75) and COF, as well as Co_3O_4 and related cobalt salts that could be formed as impurities during COF synthesis, did not give

appreciable carbon dioxide reduction (fig. S76).

To optimize this carbon dioxide catalyst platform by a modular reticular approach, we prepared the expanded COF-367-Co analog using biphenyl-4,4′-dicarboxaldehyde (BPDA) as the strut in place of BDA (Fig. 1). We reasoned that a larger pore size would allow for higher capacity of carbon dioxide adsorption inside the framework as well as higher electrochemical and chemical accessibility of the catalytic cobalt porphyrin active sites. COF-367-Co was obtained as a dark purple powder comprising rectangular rod-shaped crystallite aggregates (ca. 100 nm in length; Fig. 2D). The structural model based on PXRD data and DFT fitting indicated that the constitution and topology of COF-367-Co is analogous to that of COF-366-Co, with the former showing an increased channel width (24 Å) and interlayer distance (4.8 Å) (Fig. 2E). The BET surface area was determined by nitrogen adsorption isotherm (Fig. 2F) as 1470 m^2/g with pore size distribution consistent with the model (12 to 23 Å). Cyclic voltammetry studies with COF-367-Co on a carbon fabric electrode in bicarbonate buffer indicated that this extended organic framework exhibits an improved surface concentration of electroactive cobalt porphyrin sites over COF-366-Co of 2×10^{-9} mol/cm^2, corresponding to accessibility of 8% of the cobalt sites in the bulk material. When the solution was saturated with CO_2, a catalytic current was evident with an onset potential at −0.40 V and a 2.2-fold enhancement at −0.67 V, indicating a prominent effect of COF-367-Co in the catalysis of CO_2 reduction at these potentials (Fig. 3A). As predicted, electrolysis under the same conditions described above revealed that this expanded COF displays improved catalytic efficiency in comparison to COF-366-Co. At an applied potential of −0.67 V, COF-367-Co produced more than 100 ml carbon monoxide (STP, equivalent to 4.5 mmol) per mg of COF during a 24 hours period (TON = 3901, $TON_{EA} \approx 48{,}000$) with high Faradaic efficiency (91%). The increased TON_{EA} over COF-366-Co indicated that lattice expansion indeed allowed for more efficient exposure of the electroactive sites to the reactants.

In addition to framework expansion, we also sought to optimize catalyst performance by introducing building-block heterogeneity through a multivariate strategy (*33*), as we hypothesized that not all electroactive cobalt porphyrin sites in the material fully participated in electrocatalysis owing to the low aqueous solubility of carbon dioxide. Specifically, we reasoned that diluting electroactive cobalt porphyrin active sites within the extended lattice with isostructural metalloporphyrin units that are catalytically inactive for carbon dioxide reduction (fig. S76) could increase the proportion of the active sites exposed to the reactant and thereby improve the turnover frequency on a per cobalt basis. Copper porphyrin was chosen for this study as the corresponding COF-367-Cu had the highest surface area amongst all analogous COF-367-M synthesized (M = Ni, Zn, H_2). The resulting bimetallic COF-367 derivatives, termed COF-367-Co(10%) and COF-367-Co(1%), were prepared with the number in the parenthesis indicating the proportion of cobalt in all metal sites (Fig. 1). Indeed, ICP analyses confirmed that the final chemical composition of the COFs obtained reflected the initial ratio of the two metalloporphyrin starting materials used (section S1.1). The turnover frequency (TOF) per electroactive cobalt site for carbon monoxide production in these multivariate Co/Cu COF-367 catalysts showed a significant improvement with each 10-fold dilution of cobalt loading. The average TOF per active cobalt for the first 4 hours of reaction was measured to be: COF-367-Co: 165 $hours^{-1}$ ($TOF_{EA} \approx 1900$), COF-367-Co(10%): 360 $hours^{-1}$ ($TOF_{EA} \approx 4400$), and COF-367-Co(1%): 764 $hours^{-1}$ ($TOF_{EA} \approx 9400$) (Fig. 3C). The TOF_{EA} values were roughly estimated assuming that all three frameworks had comparable percentages of electroactive sites (8%); although the low cobalt concentration in COF-367-Co(10%) and COF-367-Co(1%) hampered the accurate determination of the surface concentration of electrochemically accessible cobalt sites by CV, the fact that the bimetallic frameworks had nearly identical pore sizes, interlayer distances and surface areas to the parent COF-367-Co on the basis of PXRD and nitrogen adsorption measurements (figs. S25 and S32 to S43) suggested that such an assumption may be valid. Owing to the moderate proton reduction ability of the copper porphyrin sites in the hybrid organic framework, the TOF increased as the Co/Cu ratio decreased at the expense of Faradaic efficiency for carbon monoxide production [FE_{CO} = 70% for COF-367-Co(10%) and 40% for COF-367-Co(1%)]. In a long-term electrolysis experiment (Fig. 3D), COF-367-Co(1%) displayed a TON of over 24,000 ($TON_{EA} \approx 296{,}000$), constituting one of the most efficient electrochemical carbon dioxide reduction catalysts reported to date (*3*, *4*). The observed activity enhancements for the bimetallic COFs are due to their unique multivariate nature; indeed, the analogous physical mixture of COF-367-Co and COF-367-Cu in a 1:9 ratio gave far less carbon dioxide reduction activity compared to COF-367-Co(10%) (table S17).

In addition to challenges posed by the low aqueous solubility and limited diffusion of CO_2 within the COF, only a small portion (4 to 8%) of the cobalt centers in the COF material deposited in this manner proved electroactive, presumably on account of the limited electrochemical contact between the COF powder and the electrode (*41*). As such, we explored the possibility of growing COF directly onto the surface of an electrode substrate in the form of oriented thin films (*42*–*44*). Layers of COF sheets could be successfully synthesized directly on glassy carbon, fluorine-doped tin oxide (FTO) and silicon oxide. Grazing incidence wide-angle X-ray scattering (GIWAXS) patterns showed the formation of highly crystalline COF thin films (figs. S48 to S51) (*45*). The concentration of COF on the substrate surface was determined using ICP to be 1.3×10^{-5} mmol Co per cm^2, corresponding to a thickness of ~350 nm, which is consistent with images obtained by cross-sectional SEM (figs. S54 and S55). The charge transport through the COF-366-Co thin

films was characterized using spectroelectrochemistry. Under an applied potential more negative than −0.37 V in nitrogen- or carbon dioxide-saturated pH 7 aqueous buffer, the UV-Vis spectrum of the FTO-supported COF underwent changes attributable to Co(II)/Co(I) reduction (Fig. 3G and figs. S78 to S82). Using the steady-state spectroscopic response to the reducing potentials in combination with the Nernst equation, the redox potential ($E_{1/2}$) could be estimated to be more negative than −0.52 V (fig. S83), in agreement with the CV measurements ($E_{1/2} \approx -0.67$ V) (*46*). The time-dependence of the UV-Vis response of a COF-coated FTO electrode to an applied potential of −0.57 V was studied in a CO_2-saturated $KHCO_3$ solution (Fig. 3G), and a fit of the data to a modified Cottrell equation afforded an apparent diffusion coefficient of 2×10^{-12} cm^2/s (fig. S81), a value substantially higher than that obtained with analogous metal-organic framework (MOF) thin films bearing cobalt porphyrin units (*47*). The direct current conductivity of COF-366-Co was also measured using the silicon oxide-hosted sample to be about 10^{-6} S/cm, also higher than that of the MOF (figs. S84 and S85). The favorable charge transport properties in addition to a presumably increased portion of electroactive cobalt sites led to a higher catalytic efficiency. Under the same electrolysis conditions, COF-366-Co thin films on glassy carbon exhibited a TOF of 665 $hours^{-1}$, a value seven times as high as that of the same material deposited on a carbon fabric, with a high current density of 45 mA/mg and a Faradaic efficiency of 86%.

Electrokinetics experiments indicated that covalently linking cobalt porphyrin active sites within a COF influences the mechanistic pathways for carbon dioxide reduction. For the systems employing COF-366-Co, COF-367-Co and COF-367-Co(10%), Tafel plots of logarithm of current density [$\log(j_{CO})$] versus overpotential (η) display comparable slopes between 470 mV/dec and 550 mV/dec in the linear, lower current density regime (−0.57 to −0.87 V), which differ significantly from what is observed for the molecular Co(TAP) analog (270 mV/dec) (Fig. 3E and figs. S65 to S68). This difference suggests that, when embedded in a structurally and electronically extended framework, cobalt porphyrin catalyzes carbon dioxide reduction by a different mechanism than pertains with the simple molecular analog. In addition, both the COF and Co(TAP) catalysts showed a first-order rate-dependence on the partial pressure of carbon dioxide (fig. S87) and no rate-dependence on the pH (figs. S88 and S89), indicating that the rate-limiting chemical step involves the participation of one molecule of carbon dioxide and no proton.

Finally, we applied X-ray absorption spectroscopy (XAS) as a probe to evaluate how the surrounding COF influenced the electronic structures of incorporated catalytic cobalt porphyrin units and in turn the associated carbon dioxide reduction mechanism (*48*, *49*). Comparison of the cobalt K-edge XAS spectra of Co(TAP), COF-367-Co and COF-367-Co(10%) (Fig. 3F) reveals a similar line size, shape and position, consistent with a formal Co(II) oxidation state for all samples. When a reducing potential was applied (−0.67 V) to COF-367-Co under a carbon dioxide atmosphere, the K-edge revealed a line shape change consistent with the partial reduction of Co(II) to Co(I) (fig. S96). The two COF catalysts also exhibited a new, additional pre-edge feature absent in the molecular Co(TAP) analog (Fig. 3F, inset); this difference shows indeed that the COF environment could directly modulate the electronic properties of molecular centers coupled into the extended lattice (*50*, *51*). This COF-unique feature was also observed when the catalysts were subjected to open-circuit or electrolysis (−0.67 V) potentials in bicarbonate buffer (figs. S92 to S95). The communication between the metal and COF lattice could furnish a cobalt center with a more delocalized electronic structure, a network-solid analog to non-innocent ligand behavior in molecular systems (*35*).

Incorporating tunable molecular units within an extended COF thus gives rise to electrocatalysts that display advantageous features of both molecular and heterogeneous systems and promote carbon dioxide reduction to carbon monoxide with exceptionally high activity and selectivity compared to existing systems (table S21). We anticipate these hybrid molecular-material platforms will be applicable to a broad range of catalytic applications, particularly those that require sustainable electrical and/or solar input and aqueous compatibility.

REFERENCES AND NOTES

1. N. S. Lewis, D. G. Nocera, Powering the planet: Chemical challenges in solar energy utilization. *Proc. Natl. Acad. Sci. U.S.A.* **103**, 15729–15735 (2006). Medline doi:10.1073/pnas.0603395103
2. H. B. Gray, Powering the planet with solar fuel. *Nat. Chem.* **1**, 7 (2009). Medline doi:10.1038/nchem.141
3. C. Costentin, M. Robert, J.-M. Savéant, Catalysis of the electrochemical reduction of carbon dioxide. *Chem. Soc. Rev.* **42**, 2423–2436 (2013). Medline doi:10.1039/C2CS35360A
4. B. Kumar, M. Llorente, J. Froehlich, T. Dang, A. Sathrum, C. P. Kubiak, Photochemical and photoelectrochemical reduction of CO_2. *Annu. Rev. Phys. Chem.* **63**, 541–569 (2012). Medline doi:10.1146/annurev-physchem-032511-143759
5. A. M. Appel, J. E. Bercaw, A. B. Bocarsly, H. Dobbek, D. L. DuBois, M. Dupuis, J. G. Ferry, E. Fujita, R. Hille, P. J. Kenis, C. A. Kerfeld, R. H. Morris, C. H. Peden, A. R. Portis, S. W. Ragsdale, T. B. Rauchfuss, J. N. Reek, L. C. Seefeldt, R. K. Thauer, G. L. Waldrop, Frontiers, opportunities, and challenges in biochemical and chemical catalysis of CO_2 fixation. *Chem. Rev.* **113**, 6621–6658 (2013). Medline doi:10.1021/cr300463y
6. B. Fisher, R. Eisenberg, Electrocatalytic reduction of carbon dioxide by using macrocycles of nickel and cobalt. *J. Am. Chem. Soc.* **102**, 7361–7363 (1980). doi:10.1021/ja00544a035
7. J. Hawecker, J.-M. Lehn, R. Ziessel, Electrocatalytic reduction of carbon dioxide mediated by $Re(bipy)(CO)_3Cl$ (bipy = 2,2′-bipyridine). *J. Chem. Soc. Chem. Commun.* **1984**, 328–330 (1984). doi:10.1039/c39840000328
8. M. Beley, J. P. Collin, R. Ruppert, J. P. Sauvage, Electrocatalytic reduction of carbon dioxide by nickel $cyclam^{2+}$ in water: Study of the factors affecting the efficiency and the selectivity of the process. *J. Am. Chem. Soc.* **108**, 7461–7467 (1986). Medline doi:10.1021/ja00284a003
9. E. B. Cole, P. S. Lakkaraju, D. M. Rampulla, A. J. Morris, E. Abelev, A. B. Bocarsly, Using a one-electron shuttle for the multielectron reduction of CO_2 to methanol: Kinetic, mechanistic, and structural insights. *J. Am. Chem. Soc.* **132**, 11539–11551 (2010). Medline doi:10.1021/ja1023496
10. M. Bourrez, F. Molton, S. Chardon-Noblat, A. Deronzier, $[Mn(bipyridyl)(CO)_3Br]$:

An abundant metal carbonyl complex as efficient electrocatalyst for CO_2 reduction. *Angew. Chem. Int. Ed.* **50**, 9903–9906 (2011). doi:10.1002/anie.201103616
11. J. Schneider, H. Jia, K. Kobiro, D. E. Cabelli, J. T. Muckerman, E. Fujita, Nickel(II) macrocycles: Highly efficient electrocatalysts for the selective reduction of CO_2 to CO. *Energy Environ. Sci.* **5**, 9502–9510 (2012). doi:10.1039/c2ee22528j
12. V. S. Thoi, N. Kornienko, C. G. Margarit, P. Yang, C. J. Chang, Visible-light photoredox catalysis: Selective reduction of carbon dioxide to carbon monoxide by a nickel N-heterocyclic carbene-isoquinoline complex. *J. Am. Chem. Soc.* **135**, 14413–14424 (2013). Medline doi:10.1021/ja4074003
13. P. Kang, T. J. Meyer, M. Brookhart, Selective electrocatalytic reduction of carbon dioxide to formate by a water-soluble iridium pincer catalyst. *Chem. Sci.* **4**, 3497–3502 (2013). doi:10.1039/c3sc51339d
14. B. A. Rosen, A. Salehi-Khojin, M. R. Thorson, W. Zhu, D. T. Whipple, P. J. Kenis, R. I. Masel, Ionic liquid-mediated selective conversion of CO_2 to CO at low overpotentials. *Science* **334**, 643–644 (2011). Medline
15. K. P. Kuhl, E. R. Cave, D. N. Abram, T. F. Jaramillo, New insights into the electrochemical reduction of carbon dioxide on metallic copper surfaces. *Energy Environ. Sci.* **5**, 7050–7059 (2012). doi:10.1039/c2ee21234j
16. C. W. Li, M. W. Kanan, CO_2 reduction at low overpotential on Cu electrodes resulting from the reduction of thick Cu_2O films. *J. Am. Chem. Soc.* **134**, 7231–7234 (2012). Medline doi:10.1021/ja3010978
17. W. Zhu, R. Michalsky, Ö. Metin, H. Lv, S. Guo, C. J. Wright, X. Sun, A. A. Peterson, S. Sun, Monodisperse Au nanoparticles for selective electrocatalytic reduction of CO_2 to CO. *J. Am. Chem. Soc.* **135**, 16833–16836 (2013). Medline doi:10.1021/ja409445p
18. D. Kim, J. Resasco, Y. Yu, A. M. Asiri, P. Yang, Synergistic geometric and electronic effects for electrochemical reduction of carbon dioxide using gold-copper bimetallic nanoparticles. *Nat. Commun.* **5**, 4948 (2014). Medline doi:10.1038/ncomms5948
19. S. Zhang, P. Kang, T. J. Meyer, Nanostructured tin catalysts for selective electrochemical reduction of carbon dioxide to formate. *J. Am. Chem. Soc.* **136**, 1734–1737 (2014). Medline doi:10.1021/ja4113885
20. A. P. Côté, A. I. Benin, N. W. Ockwig, M. O'Keeffe, A. J. Matzger, O. M. Yaghi, Porous, crystalline, covalent organic frameworks. *Science* **310**, 1166–1170 (2005). Medline doi:10.1126/science.1120411
21. E. L. Spitler, W. R. Dichtel, Lewis acid-catalysed formation of two-dimensional phthalocyanine covalent organic frameworks. *Nat. Chem.* **2**, 672–677 (2010). Medline doi:10.1038/nchem.695
22. S. Wan, F. Gándara, A. Asano, H. Furukawa, A. Saeki, S. K. Dey, L. Liao, M. W. Ambrogio, Y. Y. Botros, X. Duan, S. Seki, J. F. Stoddart, O. M. Yaghi, Covalent organic frameworks with high charge carrier mobility. *Chem. Mater.* **23**, 4094–4097 (2011). doi:10.1021/cm201140r
23. H. M. El-Kaderi, J. R. Hunt, J. L. Mendoza-Cortés, A. P. Côté, R. E. Taylor, M. O'Keeffe, O. M. Yaghi, Designed synthesis of 3D covalent organic frameworks. *Science* **316**, 268–272 (2007). Medline doi:10.1126/science.1139915
24. E. L. Spitler, J. W. Colson, F. J. Uribe-Romo, A. R. Woll, M. R. Giovino, A. Saldivar, W. R. Dichtel, Lattice expansion of highly oriented 2D phthalocyanine covalent organic framework films. *Angew. Chem. Int. Ed.* **51**, 2623–2627 (2012). doi:10.1002/anie.201107070
25. W. Lu, Z. Wei, Z. Y. Gu, T. F. Liu, J. Park, J. Park, J. Tian, M. Zhang, Q. Zhang, T. Gentle III, M. Bosch, H. C. Zhou, Tuning the structure and function of metal-organic frameworks via linker design. *Chem. Soc. Rev.* **43**, 5561–5593 (2014). Medline doi:10.1039/C4CS00003J
26. D. N. Bunck, W. R. Dichtel, Internal functionalization of three-dimensional covalent organic frameworks. *Angew. Chem. Int. Ed.* **51**, 1885–1889 (2012). doi:10.1002/anie.201108462
27. L. Ma, J. M. Falkowski, C. Abney, W. Lin, A series of isoreticular chiral metal-organic frameworks as a tunable platform for asymmetric catalysis. *Nat. Chem.* **2**, 838–846 (2010). Medline doi:10.1038/nchem.738
28. J. Lee, O. K. Farha, J. Roberts, K. A. Scheidt, S. T. Nguyen, J. T. Hupp, Metal-organic framework materials as catalysts. *Chem. Soc. Rev.* **38**, 1450–1459 (2009). Medline doi:10.1039/b807080f
29. J. Park, D. Feng, H.-C. Zhou, Structure-assisted functional anchor implantation in robust metal-organic frameworks with ultralarge pores. *J. Am. Chem. Soc.* **137**, 1663–1672 (2015). Medline doi:10.1021/ja5123528
30. D. J. Xiao, E. D. Bloch, J. A. Mason, W. L. Queen, M. R. Hudson, N. Planas, J. Borycz, A. L. Dzubak, P. Verma, K. Lee, F. Bonino, V. Crocellà, J. Yano, S. Bordiga, D. G. Truhlar, L. Gagliardi, C. M. Brown, J. R. Long, Oxidation of ethane to ethanol by N_2O in a metal-organic framework with coordinatively unsaturated iron(II) sites. *Nat. Chem.* **6**, 590–595 (2014). Medline doi:10.1038/nchem.1956
31. C. Wang, Z. Xie, K. E. deKrafft, W. Lin, Doping metal-organic frameworks for water oxidation, carbon dioxide reduction, and organic photocatalysis. *J. Am. Chem. Soc.* **133**, 13445–13454 (2011). Medline doi:10.1021/ja203564w
32. S. Pullen, H. Fei, A. Orthaber, S. M. Cohen, S. Ott, Enhanced photochemical hydrogen production by a molecular diiron catalyst incorporated into a metal-organic framework. *J. Am. Chem. Soc.* **135**, 16997–17003 (2013). Medline doi:10.1021/ja407176p
33. H. Deng, C. J. Doonan, H. Furukawa, R. B. Ferreira, J. Towne, C. B. Knobler, B. Wang, O. M. Yaghi, Multiple functional groups of varying ratios in metal-organic frameworks. *Science* **327**, 846–850 (2010). Medline doi:10.1126/science.1181761
34. D. Behar, T. Dhanasekaran, P. Neta, C. M. Hosten, D. Ejeh, P. Hambright, E. Fujita, Cobalt porphyrin catalyzed reduction of CO_2. Radiation chemical, photochemical, and electrochemical studies. *J. Phys. Chem. A* **102**, 2870–2877 (1998). doi:10.1021/jp9807017
35. R. Eisenberg, H. B. Gray, Noninnocence in metal complexes: A dithiolene dawn. *Inorg. Chem.* **50**, 9741–9751 (2011). Medline doi:10.1021/ic2011748
36. G. H. V. Bertrand, V. K. Michaelis, T. C. Ong, R. G. Griffin, M. Dincă, Thiophene-based covalent organic frameworks. *Proc. Natl. Acad. Sci. U.S.A.* **110**, 4923–4928 (2013). Medline doi:10.1073/pnas.1221824110
37. J. Guo, Y. Xu, S. Jin, L. Chen, T. Kaji, Y. Honsho, M. A. Addicoat, J. Kim, A. Saeki, H. Ihee, S. Seki, S. Irle, M. Hiramoto, J. Gao, D. Jiang, Conjugated organic framework with three-dimensionally ordered stable structure and delocalized π clouds. *Nat. Commun.* **4**, 2736 (2013). Medline doi:10.1038/ncomms3736
38. M. Calik, F. Auras, L. M. Salonen, K. Bader, I. Grill, M. Handloser, D. D. Medina, M. Dogru, F. Löbermann, D. Trauner, A. Hartschuh, T. Bein, Extraction of photogenerated electrons and holes from a covalent organic framework integrated heterojunction. *J. Am. Chem. Soc.* **136**, 17802–17807 (2014). Medline doi:10.1021/ja509551m
39. In pH 7.2 phosphate buffer, electrolyses at potentials equal to or more negative than −0.67 V resulted in moderate hydrogen evolution reactivity. This activity was however largely suppressed when the solution was saturated with carbon dioxide (vide infra).
40. The intrinsic i_{cat}/i_p value was likely higher as under carbon dioxide atmosphere, the current resulting from proton reduction was inhibited.
41. C. R. DeBlase, K. Hernández-Burgos, K. E. Silberstein, G. G. Rodríguez-Calero, R. P. Bisbey, H. D. Abruña, W. R. Dichtel, Rapid and efficient redox processes within 2D covalent organic framework thin films. *ACS Nano* **9**, 3178–3183 (2015). Medline doi:10.1021/acsnano.5b00184
42. J. W. Colson, A. R. Woll, A. Mukherjee, M. P. Levendorf, E. L. Spitler, V. B. Shields, M. G. Spencer, J. Park, W. R. Dichtel, Oriented 2D covalent organic framework thin films on single-layer graphene. *Science* **332**, 228–231 (2011). Medline doi:10.1126/science.1202747
43. D. D. Medina, V. Werner, F. Auras, R. Tautz, M. Dogru, J. Schuster, S. Linke, M. Döblinger, J. Feldmann, P. Knochel, T. Bein, Oriented thin films of a benzodithiophene covalent organic framework. *ACS Nano* **8**, 4042–4052 (2014). Medline doi:10.1021/nn5000223
44. X.-H. Liu, C. Z. Guan, S. Y. Ding, W. Wang, H. J. Yan, D. Wang, L. J. Wan, On-surface synthesis of single-layered two-dimensional covalent organic frameworks via solid-vapor interface reactions. *J. Am. Chem. Soc.* **135**, 10470–10474 (2013). Medline doi:10.1021/ja403464h
45. The COF-coated glassy carbon showed an ill-defined GIWAXS pattern due to high background scattering (figs. S52 and S53). Because the synthetic conditions were identical to those used with FTO and silicon oxide, we assumed that the COF grown on glassy carbon also formed a crystalline thin film.
46. $E_{1/2}$ could not be accurately measured using this method due to decomposition of FTO at potentials more negative than −0.57 V.
47. S. R. Ahrenholtz, C. C. Epley, A. J. Morris, Solvothermal preparation of an electrocatalytic metalloporphyrin MOF thin film and its redox hopping charge-transfer mechanism. *J. Am. Chem. Soc.* **136**, 2464–2472 (2014). Medline doi:10.1021/ja410684q
48. A. A. Peterson, J. K. Nørskov, Activity descriptors for CO_2 electroreduction to methane on transition-metal catalysts. *J. Phys. Chem. Lett.* **3**, 251–258 (2012). doi:10.1021/jz201461p
49. N. Kornienko, J. Resasco, N. Becknell, C. M. Jiang, Y. S. Liu, K. Nie, X. Sun, J. Guo,

S. R. Leone, P. Yang, Operando spectroscopic analysis of an amorphous cobalt sulfide hydrogen evolution electrocatalyst. *J. Am. Chem. Soc.* **137**, 7448–7455 (2015). Medline doi:10.1021/jacs.5b03545
50. F. de Groot, G. Vankó, P. Glatzel, The 1s x-ray absorption pre-edge structures in transition metal oxides. *J. Phys. Condens. Matter* **21**, 104207 (2009). Medline doi:10.1088/0953-8984/21/10/104207
51. J. Yano, J. Kern, K. Sauer, M. J. Latimer, Y. Pushkar, J. Biesiadka, B. Loll, W. Saenger, J. Messinger, A. Zouni, V. K. Yachandra, Where water is oxidized to dioxygen: Structure of the photosynthetic Mn_4Ca cluster. *Science* **314**, 821–825 (2006). Medline doi:10.1126/science.1128186
52. S. A. Yao, C. B. Hansen, J. F. Berry, A convenient, high-yielding, chromatography-free method for the insertion of transition metal acetates into porphyrins. *Polyhedron* **58**, 2–6 (2013). doi:10.1016/j.poly.2012.05.038
53. W. Meng, B. Breiner, K. Rissanen, J. D. Thoburn, J. K. Clegg, J. R. Nitschke, A self-assembled M_8L_6 cubic cage that selectively encapsulates large aromatic guests. *Angew. Chem. Int. Ed.* **50**, 3479–3483 (2011). doi:10.1002/anie.201100193
54. A. K. Vannucci, L. Alibabaei, M. D. Losego, J. J. Concepcion, B. Kalanyan, G. N. Parsons, T. J. Meyer, Crossing the divide between homogeneous and heterogeneous catalysis in water oxidation. *Proc. Natl. Acad. Sci. U.S.A.* **110**, 20918–20922 (2013). Medline doi:10.1073/pnas.1319832110
55. J.-M. Savéant, *Elements of Molecular and Biomolecular Electrochemistry* (Wiley-Interscience, New York, 2006).
56. V. Iablokov, S. K. Beaumont, S. Alayoglu, V. V. Pushkarev, C. Specht, J. Gao, A. P. Alivisatos, N. Kruse, G. A. Somorjai, Size-controlled model Co nanoparticle catalysts for CO_2 hydrogenation: Synthesis, characterization, and catalytic reactions. *Nano Lett.* **12**, 3091–3096 (2012). Medline doi:10.1021/nl300973b
57. I. Bhugun, D. Lexa, J.-M. Savéant, Catalysis of the electrochemical reduction of carbon dioxide by iron(0) porphyrins: Synergystic effect of weak Brönsted acids. *J. Am. Chem. Soc.* **118**, 1769–1776 (1996). doi:10.1021/ja9534462
58. C. Costentin, G. Passard, M. Robert, J.-M. Savéant, Ultraefficient homogeneous catalyst for the CO_2-to-CO electrochemical conversion. *Proc. Natl. Acad. Sci. U.S.A.* **111**, 14990–14994 (2014). Medline doi:10.1073/pnas.1416697111
59. C. Costentin, S. Drouet, M. Robert, J.-M. Savéant, A local proton source enhances CO_2 electroreduction to CO by a molecular Fe catalyst. *Science* **338**, 90–94 (2012). Medline doi:10.1126/science.1224581
60. J. M. Smieja, C. P. Kubiak, Re(bipy-tBu)$(CO)_3$Cl-improved catalytic activity for reduction of carbon dioxide: IR-spectroelectrochemical and mechanistic studies. *Inorg. Chem.* **49**, 9283–9289 (2010). Medline doi:10.1021/ic1008363
61. M. D. Sampson, A. D. Nguyen, K. A. Grice, C. E. Moore, A. L. Rheingold, C. P. Kubiak, Manganese catalysts with bulky bipyridine ligands for the electrocatalytic reduction of carbon dioxide: Eliminating dimerization and altering catalysis. *J. Am. Chem. Soc.* **136**, 5460–5471 (2014). Medline doi:10.1021/ja501252f
62. J. D. Froehlich, C. P. Kubiak, Homogeneous CO_2 reduction by Ni(cyclam) at a glassy carbon electrode. *Inorg. Chem.* **51**, 3932–3934 (2012). Medline doi:10.1021/ic3001619
63. J. W. Raebiger, J. W. Turner, B. C. Noll, C. J. Curtis, A. Miedaner, B. Cox, D. L. DuBois, Electrochemical reduction of CO_2 to CO catalyzed by a bimetallic palladium complex. *Organometallics* **25**, 3345–3351 (2006). doi:10.1021/om060228g
64. R. J. Haines, R. E. Wittrig, C. P. Kubiak, Electrocatalytic reduction of carbon dioxide by the binuclear copper complex $[Cu_2(6\text{-(diphenylphosphino-2,2'-bipyridyl})_2(MeCN)_2][PF_6]_2$. *Inorg. Chem.* **33**, 4723–4728 (1994). doi:10.1021/ic00099a024
65. D. C. Lacy, C. C. L. McCrory, J. C. Peters, Studies of cobalt-mediated electrocatalytic CO_2 reduction using a redox-active ligand. *Inorg. Chem.* **53**, 4980–4988 (2014). Medline doi:10.1021/ic403122j
66. R. Reske, H. Mistry, F. Behafarid, B. Roldan Cuenya, P. Strasser, Particle size effects in the catalytic electroreduction of CO_2 on Cu nanoparticles. *J. Am. Chem. Soc.* **136**, 6978–6986 (2014). Medline doi:10.1021/ja500328k
67. Y. Chen, C. W. Li, M. W. Kanan, Aqueous CO_2 reduction at very low overpotential on oxide-derived Au nanoparticles. *J. Am. Chem. Soc.* **134**, 19969–19972 (2012). Medline doi:10.1021/ja309317u
68. S. Zhang, P. Kang, S. Ubnoske, M. K. Brennaman, N. Song, R. L. House, J. T. Glass, T. J. Meyer, Polyethylenimine-enhanced electrocatalytic reduction of CO_2 to formate at nitrogen-doped carbon nanomaterials. *J. Am. Chem. Soc.* **136**, 7845–7848 (2014). Medline doi:10.1021/ja5031529
69. Y. Chen, M. W. Kanan, Tin oxide dependence of the CO_2 reduction efficiency on tin electrodes and enhanced activity for tin/tin oxide thin-film catalysts. *J. Am. Chem. Soc.* **134**, 1986–1989 (2012). Medline doi:10.1021/ja2108799
70. J. Medina-Ramos, J. L. DiMeglio, J. Rosenthal, Efficient reduction of CO_2 to CO with high current density using in situ or ex situ prepared Bi-based materials. *J. Am. Chem. Soc.* **136**, 8361–8367 (2014). Medline doi:10.1021/ja501923g
71. C. E. Tornow, M. R. Thorson, S. Ma, A. A. Gewirth, P. J. A. Kenis, Nitrogen-based catalysts for the electrochemical reduction of CO_2 to CO. *J. Am. Chem. Soc.* **134**, 19520–19523 (2012). Medline doi:10.1021/ja308217w
72. B. Ravel, M. Newville, *ATHENA*, *ARTEMIS*, *HEPHAESTUS*: Data analysis for x-ray absorption spectroscopy using *IFEFFIT*. *J. Synchrotron Radiat.* **12**, 537–541 (2005). Medline doi:10.1107/S0909049505012719

ACKNOWLEDGMENTS

Financial support for energy catalysis in the C.J.C. laboratory is provided by U.S. Department of Energy/Lawrence Berkeley National Laboratory (LBNL) Grant 101528-002. Financial support for COF research in the O.M.Y. laboratory is provided by BASF SE (Ludwigshafen, Germany) for synthesis; U.S. Department of Energy, Office of Science, Office of Basic Energy Sciences, Energy Frontier Research Center grant DESC0001015 for adsorption and multivariate metallation. Financial support for energy catalysis in the P.Y. laboratory was supported by Director, Office of Science, Office of Basic Energy Sciences, Materials Science and Engineering Division, U.S. Department of Energy under Contract No. DE-AC02-05CH11231(Surface). E.M.N. acknowledges the NSF-GRFP for predoctoral fellowship. A.R.P. acknowledges the Amgen Scholar Program for support of undergraduate summer research. We thank C. Canlas (University of California, Berkeley) for the acquisition of solid-state NMR spectra, and C. Zhu at Advanced Light Source (ALS) at LBNL for the acquisition of GIWAXS data. XAS measurements were performed at the ALS. The ALS is an Office of Science User Facility operated for the U.S. DOE, Office of Science by LBNL and supported by the U.S. DOE under Contract No. DE-AC02-05CH11231. The data reported in the paper are presented in the supplementary materials.

SUPPLEMENTARY MATERIALS

www.sciencemag.org/cgi/content/full/science.aac8343/DC1
Materials and Methods
Figs. S1 to S96
Tables S1 to S21
References (*52–72*)

19 June 2015; accepted 5 August 2015
Published online 20 August 2015
10.1126/science.aac8343

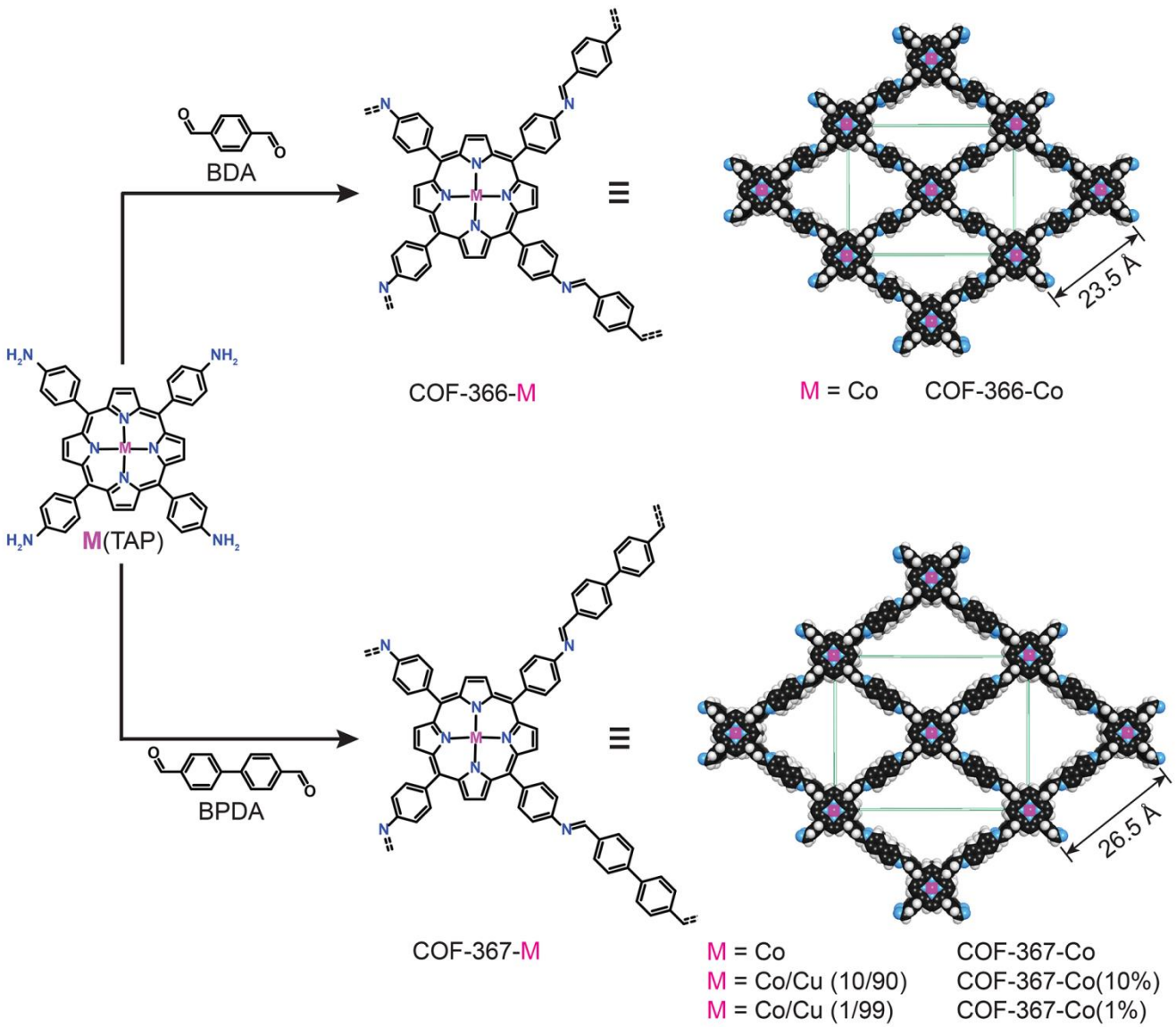

Fig. 1. Design and synthesis of metalloporphyrin-derived two-dimensional covalent organic frameworks. The space-filling structural models of COF-366-M and COF-367-M were obtained using Materials Studio 7.0 and refined with experimental PXRD data.

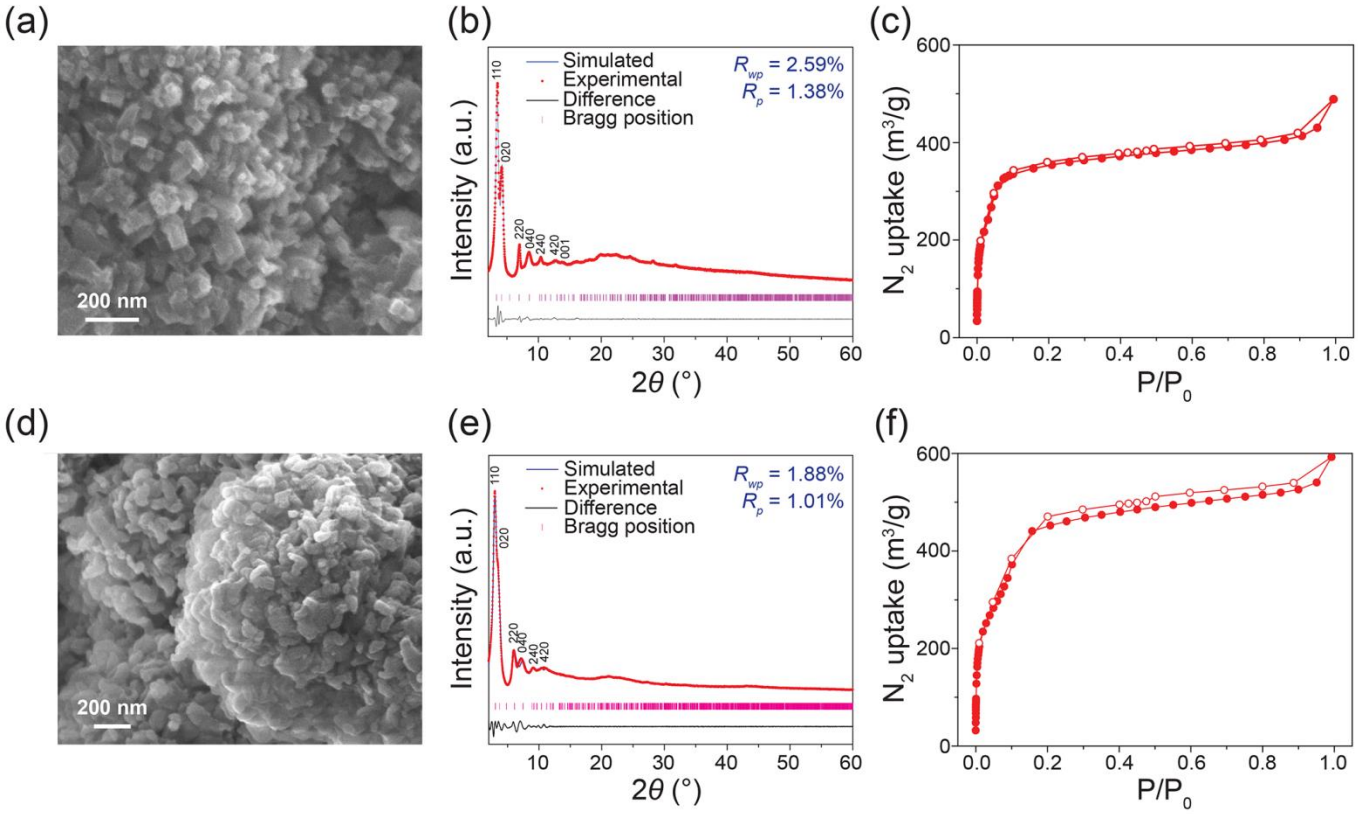

Fig. 2. Structural characterization of COF-366-Co and COF-367-Co. (**A**) SEM image of COF-366-Co. (**B**) Experimental (red line) and simulated (blue line) PXRD patterns of COF-366-Co. (**C**) Nitrogen adsorption isotherms for COF-366-Co. (**D**) SEM image of COF-367-Co. (**E**) Experimental (red line) and simulated (blue line) PXRD patterns of COF-367-Co. (**F**) Nitrogen adsorption isotherms for COF-367-Co.

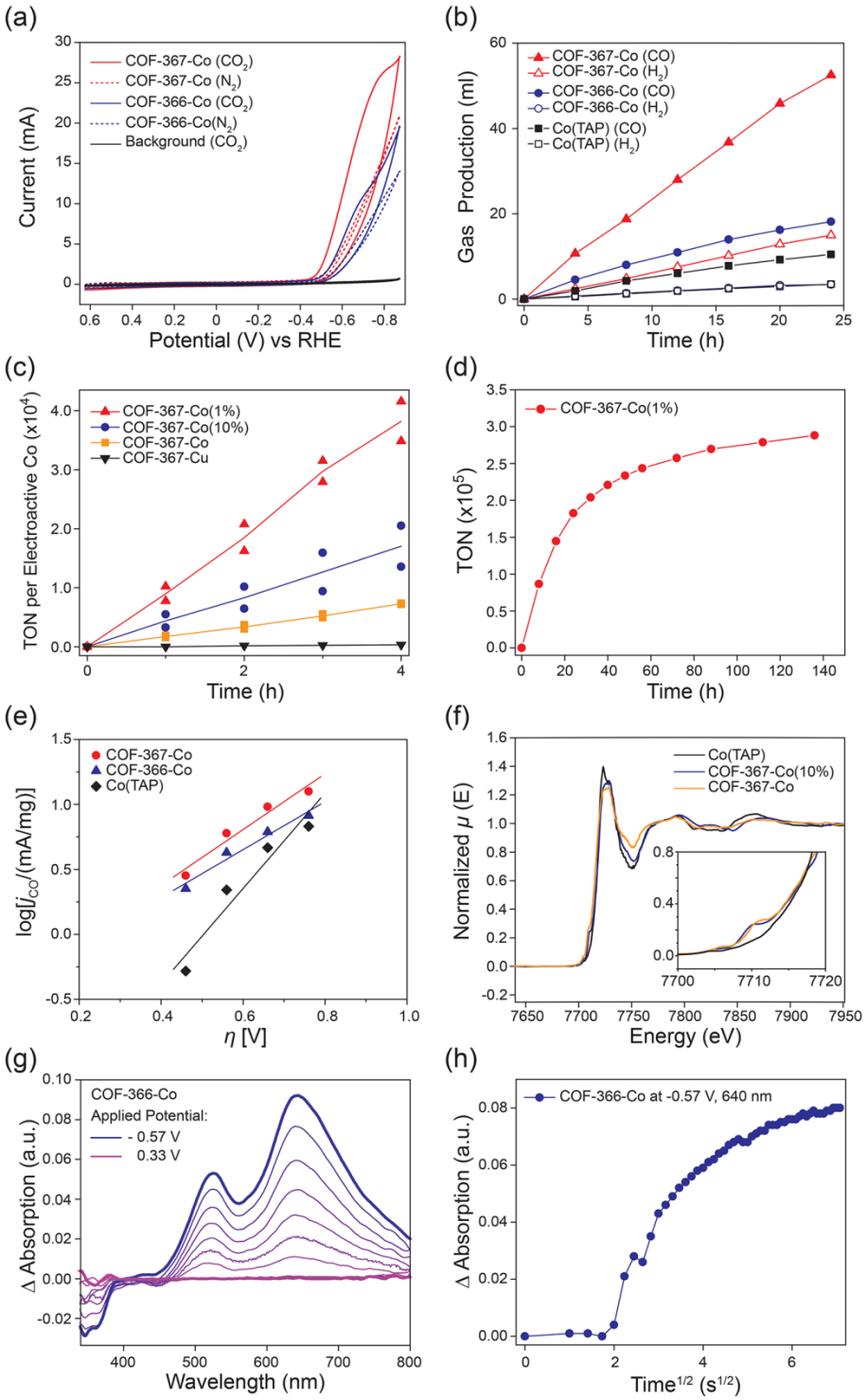
(a)
COF-367-Co (CO2)
COF-367-Co (N2)
COF-366-Co (CO2)
COF-366-Co(N2)
Background (CO2)
Current (mA)
Potential (V) vs RHE
(b)
COF-367-Co (CO)
COF-367-Co (H2)
COF-366-Co (CO)
COF-366-Co (H2)
Co(TAP) (CO)
Co(TAP) (H2)
Gas Production (ml)
Time (h)
(c)
COF-367-Co(1%)
COF-367-Co(10%)
COF-367-Co
COF-367-Cu
TON per Electroactive Co (x10^4)
Time (h)
(d)
COF-367-Co(1%)
TON (x10^5)
Time (h)
(e)
COF-367-Co
COF-366-Co
Co(TAP)
log[jCO/(mA/mg)]
η [V]
(f)
Co(TAP)
COF-367-Co(10%)
COF-367-Co
Normalized μ (E)
Energy (eV)
(g)
COF-366-Co
Applied Potential:
- 0.57 V
0.33 V
Δ Absorption (a.u.)
Wavelength (nm)
(h)
COF-366-Co at -0.57 V, 640 nm
Δ Absorption (a.u.)
Time^1/2 (s^1/2)

Fig. 3. Electrochemical/spectroelectrochemical characterizations and carbon dioxide reduction performance of the COFs. (**A**) Cyclic voltammograms of COF-366-Co and COF-367-Co in carbon dioxide-saturated medium (blue and red solid lines, respectively) or nitrogen-saturated medium (blue and red dotted lines, respectively), and background (bare carbon electrode) CV responses in carbon dioxide-saturated medium (black solid line). The medium was pH 7.2 aqueous potassium phosphate buffer (0.2 M) with additives: 0.5 M $KHCO_3$ under carbon dioxide atmosphere to maintain a neutral pH, or 0.5 M $NaClO_4$ under nitrogen atmosphere to match the ionic strength. (**B**) Long-term bulk electrolyses at −0.67 V (versus RHE) showing volume of carbon monoxide produced by COF-367-Co (red filled triangles), COF-366-Co (blue filled circles), or Co(TAP) (black filled squares), and volume of hydrogen produced by COF-367-Co (red empty triangles), COF-366-Co (blue empty circles), or Co(TAP) (black empty squares). (**C**) Bulk electrolyses of bimetallic COFs at −0.67 V (versus RHE), showing TON of carbon monoxide production by COF-367-Co(1%) (red filled triangles), COF-367-Co(10%) (blue filled circles), COF-367-Co (orange filled squares), or COF-367-Cu (purple filled inverted triangle, TON with respect to the amount of copper porphyrin). Two separate experimental runs were conducted for each time point, with the line showing the average of the measurements. (**D**) Long-term bulk electrolysis of COF-367-Co(1%) at −0.67 V (versus RHE, red filled circles). (**E**) Tafel plots of electrolysis using COF-367-Co (red filled circles), COF-366-Co (blue filled triangles), or Co(TAP) (black filled diamonds), showing only the linear, low current density regime where reaction rate is not limited by mass transport. (**F**) X-ray absorption spectra of COF-367-Co (orange line), COF-367-Co(10%) (blue line), and Co(TAP) (black line), with the inset showing the pre-edge regime of the same spectra. (**G**) Spectroelectrochemical data using in-situ UV-Vis, showing the steady-state relative absorbance at different applied potentials (0.23 V to −0.57 V versus RHE) with reference to that at 0.33 V. (**H**) Time-dependence of the relative UV-Vis absorbance at 640 nm wavelength at −0.57 V with respect to the steady-state UV-Vis absorbance at 640 nm at 0.33 V. Potential is applied at four seconds. Linear regression yielded the apparent diffusion coefficient (D_{app}) according to a modified Cottrell equation: $\Delta Absorption = \frac{2A_{\max}D_{app}^{1/2}t^{1/2}}{d\pi^{1/2}}$ (fig. S81) (*47*). Here, A_{max} is the maximum absorption of the thin films at 640 nm, d is the overall thickness of the thin films.